2013-11-21

# *High Surface Area Carbon Nanofibers Derived from Electrospun PIM-1 for Energy Storage Applications*

UTD AUTHOR(S): Jeliza S. Bonso, Grace Jones D. Kalaw and John P. Ferraris

Journal of Materials Chemistry A

PAPER

View Article Online
View Journal | View Issue

# High surface area carbon nanofibers derived from electrospun PIM-1 for energy storage applications†

Cite this: J. Mater. Chem. A, 2014, 2, 418

Jeliza S. Bonso,[a] Grace D. Kalaw[a] and John P. Ferraris*[ab]

Electrochemical double layer capacitors (EDLCs) utilize electrodes with high surface area to achieve high-energy storage capability. In this study, flexible and freestanding carbon nanofibers derived from PIM-1, a microporous polymer with high free volume, were prepared by pyrolysis of the electrospun polymer. A BET surface area of 546 $m^2$ $g^{-1}$ was obtained upon carbonization of the electrospun PIM-1 fibers. After further heat treatments such as steam-activation and annealing, the surface area increased to 1162 $m^2$ $g^{-1}$. These carbon fibers were directly used as electrodes without the use of binders in a coin cell (CR2032) configuration and were characterized by cyclic voltammetry, galvanostatic charge–discharge and electrochemical impedance spectroscopy. The activated and annealed fibers gave a specific capacitance of 120 F $g^{-1}$ at a scan rate of 10 mV $s^{-1}$ using 1,3-ethylmethylimidizaolium bis(trifluoromethanesulfonyl)imide as the ionic liquid electrolyte. From the galvanostatic charge–discharge test, the supercapacitor exhibited energy and power densities of 60 W h $kg^{-1}$ (active material) and 1.7 kW $kg^{-1}$, respectively, at a current density of 1 A $g^{-1}$. High power application of this device was demonstrated by its 77% retention of the energy density (47 W h $kg^{-1}$) at a higher discharge current density of 5 A $g^{-1}$.

Received 20th September 2013
Accepted 9th November 2013

DOI: 10.1039/c3ta13779a

www.rsc.org/MaterialsA

## Introduction

Energy storage devices that are capable of delivering large amounts of energy at high discharge rates are desirable in applications such as hybrid electric vehicles (HEV), load-levelling devices and other peak power systems.[1] Supercapacitors can be suitable for these applications because they possess energy and power densities that are intermediate to batteries and conventional capacitors. They also have higher coulombic efficiency, longer cycle life and wider working potential, albeit at lower overall energy density, than batteries.[2,3] Electrochemical double layer capacitors (EDLCs) are supercapacitors that utilize carbon-based materials such as activated carbon, carbon aerogels, carbon nanotubes and graphene, as electrodes.[4–8] They are advantageous over pseudocapacitors (conducting polymers or metal oxides) in terms of cost, power, electrical conductivity and mechanical stability, although they generally have lower energy densities.[9,10] EDLCs store charge *via* the electrostatic interaction between the electrode and the electrolyte ions when a potential difference is applied between the device's electrodes.[11] Therefore, the amount of energy stored by EDLCs is dependent on the surface area of the electrodes available for electrolyte access. Commercial supercapacitors utilize activated carbon as the electrodes. Carbon fibers are a good candidate for supercapacitors because of their mechanical strength, good electrical conductivity and the capability to be used directly without the use of binders, which can decrease the overall porosity and conductivity of the electrodes.[12]

Electrospinning is a versatile technique for producing continuous fibers with controllable diameters ranging from micron to nanometer scale.[13] Generally, the fibers are obtained from a precursor polymer solution or a polymer melt. The precursor is usually loaded in a syringe with a charged needle tip (usually 10–20 kV) from which fibers are extruded to a grounded collector.[14] The obtained fiber mat can be pyrolyzed to obtain carbon fibers. Polyacrylonitrile, polybenzimidazole and polyimides have been reported to be good precursors for carbon nanofibers that are characterized by good electrical conductivity and tensile strength.[15–17] Carbonized fibers from these polymers, however, have low surface area due to polymer chain packing during heat treatment. To make them suitable as supercapacitor electrodes, their surface area is usually increased by the addition of pore-forming agents (porogens), pore-templating agents, or the addition of sacrificial polymers that eventually decompose and introduce pores on the fibers.[18–21] These techniques pose considerations such as polymer compatibility, uniformity of dispersion, and post-treatment conditions to remove inorganic salts that may have evolved.

[a]Department of Chemistry, The University of Texas at Dallas, 800 W. Campbell Road, Richardson, TX 75080, US. E-mail: ferraris@utdallas.edu; Fax: +1 972-883-2925; Tel: +1 972-883-2901

[b]The Alan G. MacDiarmid NanoTech Institute, The University of Texas at Dallas, 800 W. Campbell Road, Richardson, TX 75080, US

† Electronic supplementary information (ESI) available: See DOI: 10.1039/c3ta13779a

In this study, we prepared flexible, high surface area carbon electrodes obtained by electrospinning a porous polymer precursor. PIM-1, or polymer of intrinsic microporosity, is a polymer with a high fractional free-volume (26%) and reported to have a BET surface area of 760 $m^2 g^{-1}$.[22] It is a rigid polymer due to the fused ring structure that prevents rotation and packing even at elevated temperature, a feature that can be utilized to obtain porous carbon. Electrospinning of PIM-1 was carried out to obtain a flexible and freestanding fiber mat, then thermally treated and used directly as electrodes for supercapacitors. An ionic liquid electrolyte, 1,3-ethylmethylimidazolium bis(trufluoromethylsulfonyl)imide (EMITFSI) was used to achieve a working potential of 3.5 V. High energy density with high capacitance retention was observed from the porous carbon nanofiber electrodes derived from PIM-1.

# Experimental

### Materials

Potassium carbonate (99.5% purity), 2,3,5,6-tetrafluoroterepthalonitrile (99% purity, TFPN), and anhydrous *N*,*N*′-dimethylformamide (DMF) were purchased from Sigma Aldrich and used as received. 3,3,3′,3′-tetramethyl-1,1′-spirobisindane-5,5′,6,6′-tetrol (97% purity, TTSBI) powder was purified by recrystallization using methanol/dichloromethane and dried at 60 °C under vacuum prior to use. Electrochemical grade EMITFSI (99.5% purity) was purchased from IoLiTec, Inc. and was used without further purification. The coin cell assembly parts were obtained from Shenzhen Yongxingye Precision Machinery Mould Co. Ltd., China.

### Synthesis of PIM-1

PIM-1 was synthesized by following reported literature procedures.[23] Briefly, the freshly purified TTSBI and TFPN (1 : 1 molar ratio) were mixed in DMF at 70 °C for 72 h under a nitrogen blanket. The reaction was terminated by the addition of THF. The polymer was precipitated and washed with methanol, then dried in a vacuum oven prior to use.

### Electrospinning and thermal treatments

A 10 wt% solution of PIM-1 in tetrachloroethane was prepared by stirring the mixture at room temperature. To carry out the electrospinning process, the obtained solution was placed in a syringe and ejected through a needle charged with a potential of 10–15 kV at a feed rate of 1–2 ml $h^{-1}$ and collected in a grounded collector that rotates at 300 rpm. The obtained fiber mat was carbonized at 1000 °C at a ramp rate of 5 °C $min^{-1}$ and dwelled for 1 h under nitrogen flow. To further improve the surface area of the carbon fibers, activation with steam was carried out at 800 °C for 1 h. The steam was obtained by flowing nitrogen through a custom-built steam-generator supplied with water by an HPLC pump at a rate of 5 ml $h^{-1}$. A final annealing treatment was done at 900 °C under nitrogen.

### Characterization

The synthesized PIM-1 was characterized by proton NMR ($^1$H NMR) and attenuated total reflectance Fourier transform infrared (ATR-FTIR) spectroscopy. Nuclear magnetic resonance (NMR) was acquired in $CDCl_3$ with TMS ($^1$H) as internal standard on a Bruker AVANCE III™ (500 MHz). The molecular weight of PIM-1 was obtained *via* gel permeation chromatography (GPC) using two ViscoGEL columns in series (I-MBHMW 3078, Viscotek) with THF as the eluting solvent at a flow rate of 1 ml $min^{-1}$, and a Triple Detector SEC system (Module TDA 320, Viscotek). Thermal properties were analyzed using a TA Instruments SDT Q600 Analyzer. The morphology and fiber diameter of the electrospun PIM-1 before and after thermal treatments were studied using a Zeiss Supra™ 40 variable-pressure field-effect scanning electron microscope. The presence of graphitic and amorphous carbons was determined using a JobinYvon HORIBA LabRam Raman spectrometer equipped with a 633 nm He–Ne laser. Surface area and pore size distribution by nitrogen adsorption/desorption were measured using a Quantachrome Instruments Autosorb-1 at 77 K. The samples were degassed at 150 °C for at least 12 h prior to surface area analysis. X-ray photoelectron spectroscopy (XPS) was carried out using a monochromatic Al Kα source (1486.7 eV), pass energy of 15 eV, and an Omicron EA125 hemispherical analyzer. Peak fitting for C 1s and O 1s spectra were done using Analyzer software.

### Electrochemical tests

A coin cell (CR2032) configuration was employed to test the electrochemical performance of the obtained electrodes. The assembly, which includes two electrodes positioned on either side of a PTFE (Gore™) separator, were pressed together using a manual crimper by applying a pressure of 1000 psi. The electrodes were obtained directly from the fiber mat by punching out an area of 1 $cm^2$. Prior to obtaining measurements, the cells were cycled ten times at 10 mV $s^{-1}$ to equilibrate. Cyclic voltammetry and charge discharge tests were done using an Arbin Supercapacitor Test Station (SCTS) to assess the electrochemical performance of the electrodes. Electrochemical impedance spectroscopy was performed using a PARSTAT 2273 Galvanostat (Princeton Applied Research) at 0 V DC bias in the frequency range of 100 kHz to 10 mHz and analyzed using a PowerSuite software.

# Results and discussion

The as-synthesized PIM-1 polymer was a fluorescent yellow powder with a molecular weight ($M_w$) of 127 kDa and a narrow PDI of 1.96. The structure and purity of the polymer were confirmed by $^1$H-NMR and ATR-FTIR spectra (Fig. S1 and S2†). Thermogravimetric analysis of the PIM-1 fibers (Fig. 1) shows that decomposition occurs at 478 °C (5% weight loss) with a char yield of ~45% at 1000 °C, which is similar to high char yield polymers such as polyacrylonitrile and various polyamides.[24,25] The DTG curve shows a peak at 498 °C, in which weight loss is at its maximum. Fig. 2 shows the optical images of

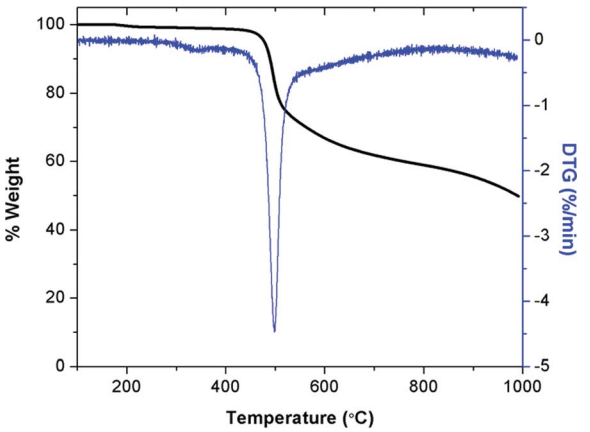


Fig. 1 TGA–DTG curve of PIM-1 fibers at 5 °C $min^{-1}$ under nitrogen flow.

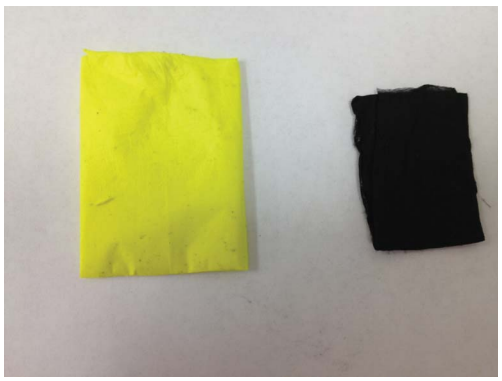

Fig. 2 Optical images of the as-spun (left) and carbonized (right) PIM-1 fibers.

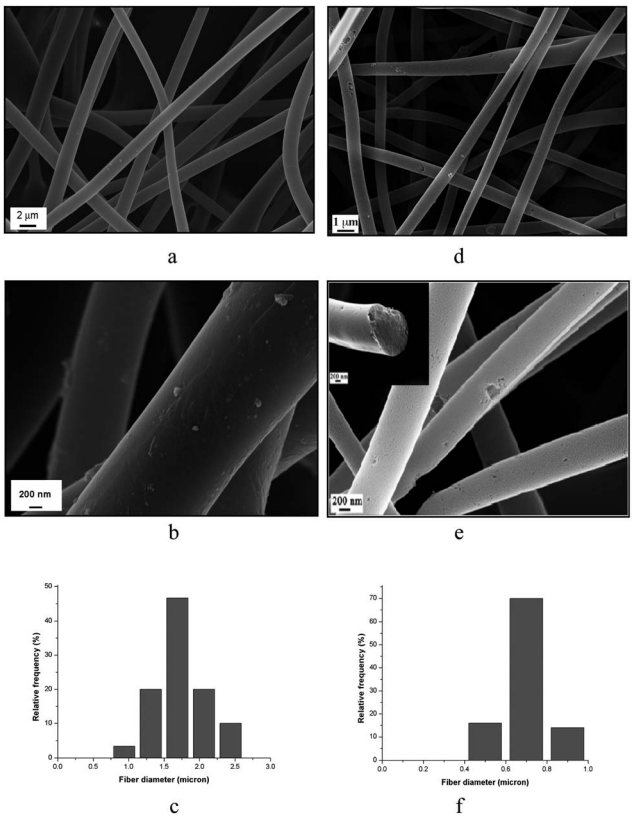


Fig. 3 SEM images of (a and b) electrospun and (d and e) carbonized PIM-1; fiber diameter distribution of (c) electrospun and (f) carbonized PIM-1.

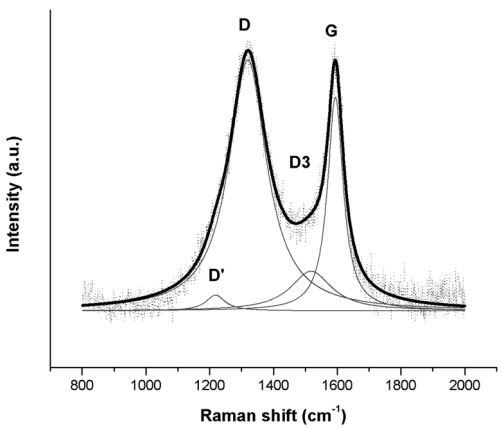


Fig. 4 Deconvoluted Raman spectrum of carbonized PIM-1.

the yellow electrospun PIM-1 mat and the resulting carbonized fibers, which retained flexibility. The SEM images (Fig. 3) of the electrospun PIM-1 and the resulting carbon nanofibers (CNFs) show uniform and bead-free fibers. The electrospun PIM-1 fibers have an average diameter of 1.7 ± 0.3 microns. After thermal treatments (carbonization, activation and annealing), the fiber structure was retained and the diameter decreased to submicron range (697 ± 86 nm). It can be also observed that the surface of the carbonized fibers has a rougher texture. The Raman spectrum of the CNFs in Fig. 4 shows peaks at 1315 $cm^{-1}$ and 1590 $cm^{-1}$, corresponding to the D and G bands, respectively. The D band is mainly due to the disordered and/or amorphous $sp^3$ carbon while the G band is characteristic of graphitic carbon.[26] The spectrum was deconvoluted using OriginPro 8.0 into four Lorentzian peaks to reveal additional peaks at 1169 $cm^{-1}$ ($D_4$) and 1522 $cm^{-1}$ ($D_3$). The $D_4$ or I peak is attributed to the $sp^2$–$sp^3$ carbon bonds while the $D_3$ peak is associated with the presence of amorphous carbon on interstitial sites in a disturbed graphitic lattice.[27] The degree of crystallinity ($R$), which was calculated from the ratio of the integrated intensities of the D and G bands ($I_D/I_G$), is 2.32, which is typical value for carbon nanofibers from pyrolyzed polymer precursors.[28] The graphitic crystallite size ($L_a$) was 17 nm according to the modified Tuinstra–Koenig equation.[29] XPS analysis gave the surface elemental composition of the carbon nanofibers with atomic percentages of 94.8% C, 3.4% O, 0.49% N and 0.26% F. There is also a trace amount of Si that was detected and can be attributed to the quartz tube used for thermal treatments. The C 1s spectrum (Fig. 5a) shows the largest peak associated with graphitic carbon at 284.7 eV. The smaller peaks at higher binding energies can be associated with

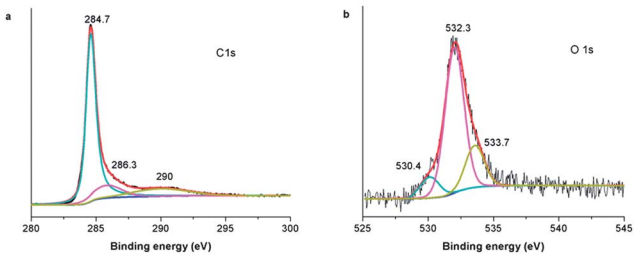


Fig. 5 Deconvoluted (a) C 1s and (b) O 1s XPS spectra of PIM-1 carbon nanofibers.

–C–O– and carbonyl carbon.[30] The deconvoluted O 1s spectrum (Fig. 5b) has the largest peak 532.3 eV which is attributed to C–OH or C–O–C. The peak at 530.4 eV can be associated with oxygen in C=O while the peak 533.7 eV is associated with moisture.[31]

The nitrogen adsorption/desorption isotherms of the carbonized only and carbonized, activated and annealed PIM-1 are shown in Fig. 6a and both can be characterized as a type II isotherm according to the International Union of Pure and Applied Chemistry (IUPAC) classification.[32] For the carbonized PIM-1, the Brunauer–Emmett–Teller (BET) specific surface area (SSA) was 546 $m^2\ g^{-1}$ and the total pore volume (TPV) was 0.287 $cm^3\ g^{-1}$. After activation and annealing, the surface area and TPV increased to 1162 $m^2\ g^{-1}$ and 0.611 $cm^3\ g^{-1}$, respectively (Table 1). The density functional theory (DFT) pore size distribution (Fig. 6b) shows the presence of micropores (<2 nm) and mesopores (2–50 nm).[33] Both the carbonized only and activated/annealed PIM-1 have pore width maxima that are <1 nm. It is noteworthy that larger pores around 1–2 nm can be observed and the relative amount of mesopores slightly increased from 20% to 23% after activation and annealing. Since the ionic liquid electrolyte used in this study have ion sizes of 4.3 × 7.6 Å (for EMI) and 2.9 × 7.9 Å (for TFSI), the increase in pore size on the fibers could facilitate better ion diffusion.[34]

Table 1 Surface area and pore size analysis data from $N_2$ sorption isotherms of carbonized and activated PIM-1 nanofibers

| | BET SSA ($m^2\ g^{-1}$) | DFT TPV ($cm^3\ g^{-1}$) | $V_{micro}$ ($cm^3\ g^{-1}$) | $V_{meso}$ ($cm^3\ g^{-1}$) |
|---|---|---|---|---|
| C1000 | 546 | 0.287 | 0.230 | 0.057 |
| C1000/SA800/AN900 | 1162 | 0.611 | 0.469 | 0.142 |

Fig. 7 shows the cyclic voltammograms (CVs) of the carbonized only (C1000) and activated/annealed (C1000/SA800/AN900) PIM-1 in EMITFSI. The capacitance, $C$, of the two-electrode device was calculated from the cyclic voltammograms using the equation:

$$C = \int I/v(\mathrm{d}t) \quad (1)$$

where $I$ is the integrated discharge current over the potential range at a particular scan rate ($v$). It should be noted that the specific capacitance, $C_{sp}$, is related to the cell capacitance as

$$C_{sp} = 4C/m \quad (2)$$

where $m$ is the mass of both electrodes and the multiplier 4 is used to obtain the specific capacitance of a single electrode since the device is considered as two capacitors in series.[35] At 10 mV $s^{-1}$, the carbonized PIM-1 supercapacitor gave a specific capacitance of 103 F $g^{-1}$ and increased to 120 F $g^{-1}$ upon activation and annealing. The shape of the CV plot is also more box-like for the activated/annealed PIM-1, which suggests better ion diffusion because of its higher surface area and larger pore size. The specific capacitance, energy and power densities can also be calculated from the constant current charge–discharge tests using the equations:[36]

$$C_{sp} = 4*(It)/(\Delta Vm) \quad (3)$$

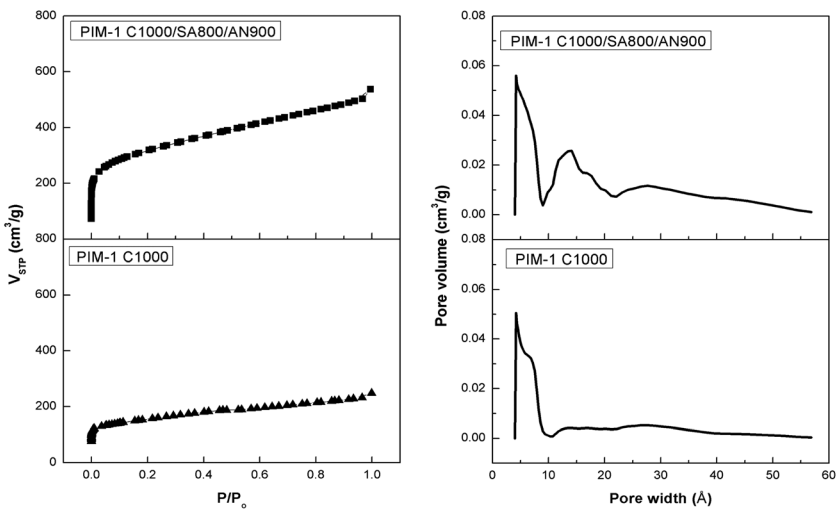


Fig. 6 Surface area and pore size analysis of carbonized and activated/annealed PIM-1 CNFs: (a) Nitrogen adsorption/desorption plot and (b) DFT pore size distribution.

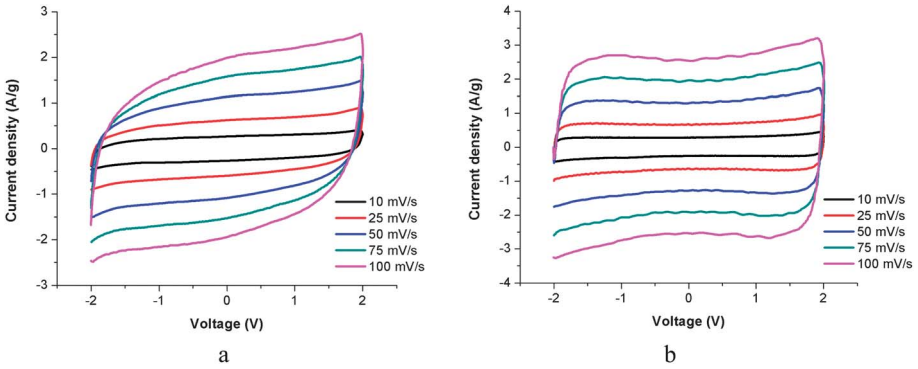


Fig. 7 Cyclic voltammograms of (a) C1000 PIM-1 and (b) C1000/SA800/AN900 PIM-1 at different scan rates.

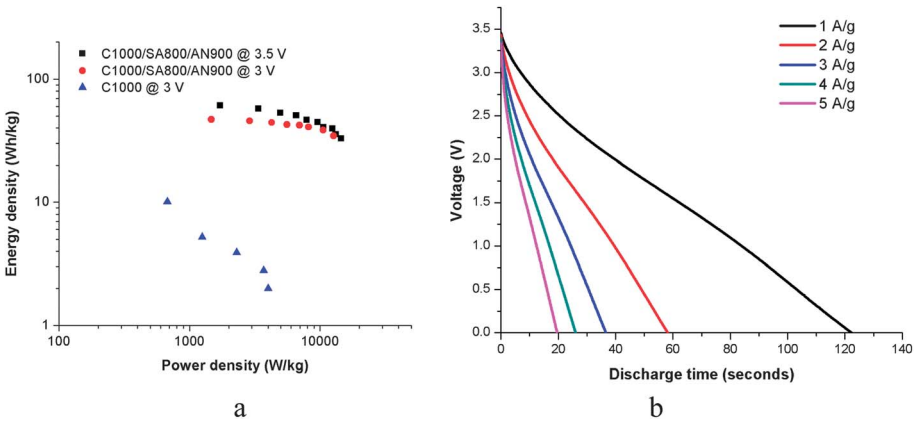


Fig. 8 (a) Ragone plot of the C1000 and C1000/SA800/AN900 and (b) discharge curves from 1–5 A $g^{-1}$ of C1000/SA800/AN900 PIM-1 carbon nanofibers.

$$E_d = 1/2C(\Delta V)^2 \quad (4)$$

$$P_d = E_d/t \quad (5)$$

where $I$ is the discharge current and $t$ is the time it takes to discharge to 0 V from the initial voltage ($\Delta V$), taking into account the IR drop at the beginning of discharge. Fig. 8a shows the Ragone plot comparing the energy and power densities of the C1000 and C1000/SA800/AN900 PIM-1 nanofibers. At a 3 V window, the energy density of the carbonized PIM-1 is 10 W h $kg^{-1}$ at 1 A $g^{-1}$. The activated/annealed PIM-1 gave a value of 46 W h $kg^{-1}$, which further increased, to 60 W h $kg^{-1}$ when the voltage window was increased to 3.5 V. Fig. 8b shows that the discharge curves for the C1000/SA800/AN900 PIM-1 are almost linear with no significant IR drop. Table 2 summarizes the electrochemical performance of the activated/annealed PIM-1 carbon nanofibers. At a high discharge current density of 10 A $g^{-1}$, more than 75% of the capacitance was retained from the 149 F $g^{-1}$ at 1 A $g^{-1}$. This demonstrates the high rate capability of the device from these carbon nanofiber electrodes derived from PIM-1.

The Nyquist plots for the C1000 and C1000/SA800/AN900 PIM-1 carbon nanofibers are shown in (Fig. 9a). The $x$-intercept in the high frequency region gives the equivalent series resistance (ESR) of 4.18 Ω for both CNFs. The ESR can be attributed mainly to the resistance of the electrolyte and the value obtained is typical for ionic liquid electrolytes like EMITFSI. At high to medium frequency region, the semi-circle observed can be related to the sum of the electrical resistance the electrolyte, contact resistance in the electrode itself and the ion transport (charge transfer) resistance of the electrolyte.[37] The diameter of the semi-circle is wider in C1000 PIM-1, which indicates that the higher surface area and larger % mesopores content on the activated and annealed carbon nanofibers allow faster diffusion of ions. Fig. 9b shows the real and imaginary

Table 2 Electrochemical performance of PIM-1 C1000/SA800/AN900 electrodes in EMITFSI

| Current density (A $g^{-1}$) | Specific capacitance (F $g^{-1}$) | Energy density (W h $kg^{-1}$) | Power density (W $kg^{-1}$) |
|---|---|---|---|
| 1 | 149 | 60 | 1715 |
| 2 | 145 | 57 | 3380 |
| 3 | 140 | 53 | 4965 |
| 4 | 135 | 51 | 6580 |
| 5 | 134 | 47 | 7900 |
| 10 | 112 | 33 | 14611 |

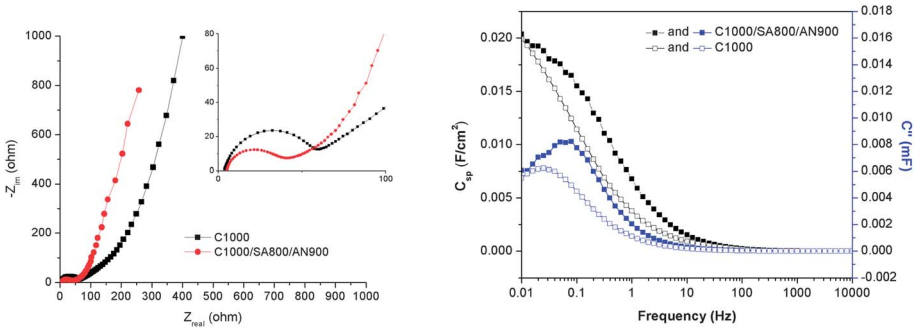


Fig. 9 (a) Nyquist plot and (b) real and imaginary capacitance *vs.* frequency plot.

capacitance values as a function of frequency. It can be seen that the C1000/SA800/AN900 PIM-1 carbon nanofibers have higher capacitance values at all frequencies. The time constant of the charge–discharge process, $\tau_o$, can be obtained from the inverse of the frequency at which the imaginary capacitance ($C''$) is at its peak ($f_o$).[38,39] For C1000, $\tau_o$ is 39.8 s while it is 4 times shorter for C1000/SA800/AN900, which is 10 s. These values reflect the rate capability of the electrodes, and thus show the activated and annealed nanofibers will provide higher power capability.

## Conclusion

Electrospinning of PIM-1 afforded uniform fibers with diameters of 1.7 micron. The electrospun PIM-1 fibers were carbonized, steam-activated and annealed to obtain a flexible, freestanding, binder-free and porous carbon fiber electrode for supercapacitors. The carbon nanofiber electrodes have submicron diameters of 600–900 nm, with an $I_D/I_G$ ratio of 2.32. The BET surface area of the carbonized PIM-1 fibers is 546 $m^2\ g^{-1}$. This demonstrates the preparation of high surface area carbon fibers from a single polymer precursor, without the use of any additive. Activation with steam caused formation of mesopores and subsequent increase in surface area to 1162 $m^2\ g^{-1}$. The activated/annealed carbon nanofibers from PIM-1 are promising electrode materials for high energy-high power applications.

## Acknowledgements

The authors gratefully acknowledge the National Science Foundation (Grant no. IIP-1127564) for financial support. We also acknowledge the NSF (CHE-1126177) grant for providing the Bruker AVANCE III™ 500 NMR facility. Help with the XPS analysis from Dr Stephen Mcdonnell and Dr Robert Wallace (Department of Materials Science and Engineering, University of Texas at Dallas), and Dr Lissa Magel (Solarno, Inc.) is also greatly appreciated.

## Notes and references

1 A. F. Burke, *Proc. IEEE*, 2007, **95**, 806–820.
2 B. E. Conway, *J. Electrochem. Soc.*, 1991, **138**, 1539–1548.
3 B. E. Conway, V. Birss and J. Wojtowicz, *J. Power Sources*, 1997, **66**, 1–14.
4 C. Portet, G. Yushin and Y. Gogotsi, *Carbon*, 2007, **45**, 2511–2518.
5 M. D. Stoller, S. Park, Y. Zhu, J. An and R. S. Ruoff, *Nano Lett.*, 2008, **8**, 3498–3502.
6 R. Signorelli, D. C. Ku, J. G. Kassakian and J. E. Schindall, *Proc. IEEE*, 2009, **97**, 1837–1847.
7 T. Bordjiba, M. Mohamedi and L. H. Dao, *Adv. Mater.*, 2008, **20**, 815–819.
8 C. G. Liu, Z. N. Yu, D. Neff, A. Zhamu and B. Z. Jang, *Nano Lett.*, 2010, **10**, 4863–4868.
9 B. E. Conway, V. Birss and J. Wojtowicz, *J. Power Sources*, 1997, **66**, 1–14.
10 C. Peng, J. Jin and G. Z. Chen, *Electrochim. Acta*, 2007, **53**, 525–537.
11 C. Largeot, C. Portet, J. Chmiola, P.-L. L. Taberna, Y. Gogotsi and P. Simon, *J. Am. Chem. Soc.*, 2008, **130**, 2730–2731.
12 C. Kim and K. S. Yang, *Appl. Phys. Lett.*, 2003, **83**, 1216–1218.
13 Z. Zhang, X. Li, C. Wang, S. Fu, Y. Liu and C. Shao, *Macromol. Mater. Eng.*, 2009, **294**, 673–678.
14 W. E. Teo and S. Ramakrishna, *Nanotechnology*, 2006, **17**, R89–R106.
15 Z.-M. Huang, Y.-Z. Zhang, M. Kotaki and S. Ramakrishna, *Compos. Sci. Technol.*, 2003, **63**, 2223–2253.
16 M. S. A. Rahaman, A. F. Ismail and A. Mustafa, *Polym. Degrad. Stab.*, 2007, **92**, 1421–1432.
17 C. Kim, *J. Power Sources*, 2005, **142**, 382–388.
18 S. K. Nataraj, B. H. Kim, C. M. Dela, J. Ferraris, T. M. Aminabhavi and K. S. Yang, *Mater. Lett.*, 2009, **63**, 218–220.
19 B. Kim, N. Bui, K. Yang, M. E. Cruz and J. P. Ferraris, *Bull. Korean Chem. Soc.*, 2009, **30**, 1967–1972.
20 K.-H. Jung and J. P. Ferraris, *Carbon*, 2012, **50**, 5309–5315.
21 C. Kim, Y. Choi, W. Lee and K. Yang, *Electrochim. Acta*, 2004, **50**, 883–887.
22 N. B. McKeown, B. Gahnem, K. J. Msayib, P. M. Budd, C. E. Tattershall, K. Mahmood, S. Tan, D. Book, H. W. Langmi and A. Walton, *Angew. Chem., Int. Ed.*, 2006, **45**, 1804–1807.
23 J. Song, N. Du, Y. Dai, G. P. Robertson, M. D. Guiver, S. Thomas and I. Pinnau, *Macromolecules*, 2008, **41**, 7411–7417.

24 A. V. Korobeinyk, R. L. D. Whitby and S. V. Mikhalovsky, *Eur. Polym. J.*, 2012, **48**, 97–104.
25 S. Xiao, B. Wang, C. Zhao, L. Xu and B. Chen, *J. Appl. Polym. Sci.*, 2013, **127**, 2332–2338.
26 M. A. Pimenta, G. Dresselhaus, M. S. Dresselhaus, L. G. Cançado, A. Jorio and R. Saito, *Phys. Chem. Chem. Phys.*, 2007, **9**, 1276–1291.
27 R. Ruiz-Rosas, J. Bedia, M. Lallave, I. G. Loscertales, A. Barrero, J. Rodríguez-Mirasol and T. Cordero, *Carbon*, 2010, **48**, 696–705.
28 Y. Wang, S. Serrano and J. J. Santiago-Aviles, *Synth. Met.*, 2003, **138**, 423–427.
29 L. G. Cançado, K. Takai, T. Enoki, M. Endo, Y. A. Kim, H. Mizusaki, A. Jorio, L. N. Coelho, R. Magalhães-Paniago and M. A. Pimenta, *Appl. Phys. Lett.*, 2006, **88**, 163106.
30 X. Feng, N. Dementev, W. Feng, R. Vidic and E. Borguet, *Carbon*, 2006, **44**, 1203–1209.
31 S. Biniak, G. Szymański, J. Siedlewski and A. ŚwiąTkowski, *Carbon*, 1997, **35**, 1799–1810.
32 K. S. W. Sing, *Pure Appl. Chem.*, 1985, **57**, 603–619.
33 D. H. Everett, *Pure Appl. Chem.*, 1972, **31**, 577–638.
34 P. Simon and Y. Gogotsi, *Nat. Mater.*, 2008, **7**, 845–854.
35 M. D. Stoller and R. S. Ruoff, *Energy Environ. Sci.*, 2010, **3**, 1294–1301.
36 L. Sun, C. Tian, M. Li, X. Meng, L. Wang, R. Wang, J. Yin and H. Fu, *J. Mater. Chem. A*, 2013, **1**, 6462.
37 T. Bordjiba, M. Mohamedi and L. Í. H. Dao, *J. Power Sources*, 2007, **172**, 991–998.
38 P. L. Taberna, P. Simon and J. F. Fauvarque, *J. Electrochem. Soc.*, 2003, **150**, A292.
39 M. Lazzari, F. Soavi and M. Mastragostino, *Fuel Cells*, 2010, **10**, 840–847.